Femtosecond time-resolved broadband electronic sum frequency generation for the investigation of electron and exciton dynamics.

L. Foglia,[1, a)] M. Wolf,[1] and J. Stähler[1, b)]
Fritz-Haber-Institut der Max-Planck-Gesellschaft, Department of Physical Chemistry, Berlin, Germany

(Dated: 1st September 2016)

Time-resolved sum-frequency generation is an established tool to investigate ultrafast vibrational dynamics with surface and interface specificity. We present an extension of the technique to the regime of electronic transitions based on a compressed white light continuum. It is used to probe the non-equilibrium dynamics of excitonic resonances in the non-centrosymmetric oxide ZnO, where we demonstrate that we can probe transient changes of the electronic sum frequency generation signal as small as 0.6%.

Second-order non-linear optical spectroscopies base on the wave-mixing phenomena that can occur in a material due to the second-order non-linear polarization

$$\mathbf{P}^{(2)}(\omega_s) = \epsilon_0 \chi^{(2)}_{eff} : \mathbf{E}(\omega_1)\mathbf{E}(\omega_2), \qquad (1)$$

acting as the source term for a third electric field $\mathbf{E}(\omega_s)$ at the sum- or difference-frequency $\omega_s = \pm\omega_1 \pm \omega_2$ as given by energy and momentum conservation[1–3]. The amplitude of this field depends on the third-rank tensor $\chi^{(2)}$, which reflects the symmetry of the material and vanishes for systems with inversion symmetry. Additionally, $\mathbf{P}^{(2)}$ is enhanced whenever at least one of the incoming or generated electric fields is resonant with an optical transition between electronic or vibrational energy levels in a material[3]. Thus, second order non-linear optical effects constitute a unique tool for the spectroscopy of electronic and vibrational states with symmetry specificity. In particular, for centrosymmetric materials and in the dipole approximation, second-order non-linear spectroscopies are intrinsically surface and interface specific, since these break the inversion symmetry[2]. Also, they are sensitive to phase transitions between centrosymmetric and non-centrosymmetric phases as well as between different non-centrosymmetric crystal structures[4]. The combination of non-linear optical spectroscopies with a third laser beam in a "pump-probe" scheme additionally allows to achieve time resolution in the femtosecond range and thereby access the ultrafast timescales of electronic and vibrational processes following photoexcitation in most materials. The sample is photoexcited by a first laser pulse, the "pump", which alters the optical and electronic properties. These pump-induced changes affect the polarization and can be monitored by the non-linear probe as a function of the time delay after photoexcitation. In this way, second-order non-linear optical effects can be used to probe the dynamics of processes such as solvation[5], molecular orientation and motion[6–9], charge and electron transfer at an interface[10–12], interfacial hybrid states[13–15] or phase transitions involving changes in symmetry[16,17].

The challenge of non-linear optical spectroscopy is that second-order susceptibilities are 9 to 11 orders of magnitude smaller than linear susceptibilities and, when aiming at time-resolved measurements, the expected pump-induced signal variation is usually 10% of this already small signal. In other words, for typical pulse energies of 1-5 μJ and at 40 kHz repetition rate, the change of the number of photons impinging on the detector is on the order of few tens of photons per second of exposure. In order to minimize the acquisition time and to optimize the signal to noise ratio and energy resolution, thus, the optimal experimental approach would be to use a broadband laser pulse as resonant field, to cover a broad region of the density of states (DOS) at once as depicted on the right of Fig. 1. This approach is routinely used to investigate vibrational dynamics in time-resolved vibrational sum frequency generation (tr-vSFG)[18,19]. Here a broadband infrared (IR) pulse, potentially resonant with vibrational transitions, is mixed with a narrowband near infrared (NIR) pulse to generate the SFG field. Ultrafast *electronic* processes in solid state samples, instead, are to date investigated using non-linear optical spectroscopy by *second harmonic* generation (SHG) only (Fig. 1

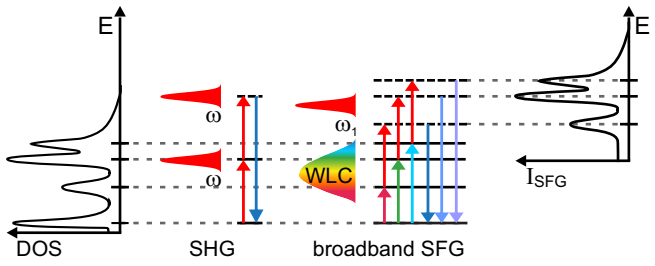

Figure 1. Simplified resonant SHG and broadband SFG scheme. The former requires the tuning of the photon energy ω to match the electronic resonance. The latter, instead, uses a broadband WLC (IR pulse) that is potentially simultaneously resonant with a series of electronic (vibrational) transitions, thus allowing for the mapping of relevant DOS at once.

[a)] Currently at Elettra Sincrotrone Trieste SCpA, Basovizza, Trieste, Italy
[b)] Electronic mail: staehler@fhi-berlin.mpg.de

left), where $\omega_1 = \omega_2 = \omega$ and $\omega_s = 2\omega$. In order to probe an electronic resonance, SHG requires to tune the laser photon energy and, thus, the spectra consist of discrete points and good energy resolution is achieved at the expense of the acquisition time. Furthermore, time-resolved SHG experiments are often performed at one particular resonance energy and are seldomly frequency-resolved[20].

In this Letter, we present an extension of time-resolved broadband sum frequency generation to the regime of *electronic* transitions for solid state samples: Time-resolved electronic sum-frequency generation (tr-eSFG). Instead of a broadband IR pulse, a white light continuum (WLC) in the visible range is upconverted by a NIR pulse ($\omega_1 = 800\,\text{nm}$) to match *electronic transitions*. This way, a wide region of the DOS is mapped at once and the energy resolution is limited by the width of the upconverting pulse only. To our knowledge, to date, this probing technique has solely been applied to the study of liquid interfaces[21]. To demonstrate the feasibility of the experiment, we tested tr-eSFG on the two non-centrosymmetric semiconductors ZnO and GaAs, where we expect relevant bulk signals due to the broken inversion symmetry. ZnO, having a wurtzite crystal structure, is chosen because it exhibits three excitonic resonances close to its 3.4 eV band gap[22] that match the eSFG energy window at $\omega_1 + \omega_2$. GaAs, which has a non-centrosymmetric zincblende structure, does not have any electronic transition resonant with ω_1, ω_2 nor with $\omega_1 + \omega_2$ and is thus used as a reference. Applying the broadband eSFG approach, we are able to identify all ZnO excitonic resonances and their dynamics with 160 fs time resolution, detecting pump-induced changes as low as 0.6 %.

Fig. 2 shows the experimental setup. We used a commercial, regeneratively amplified femtosecond (Ti:Sa) laser system (Coherent RegA) working at 40 kHz repetition rate, providing 800 nm light pulses of 40 fs duration. Half of the output power is used to generate

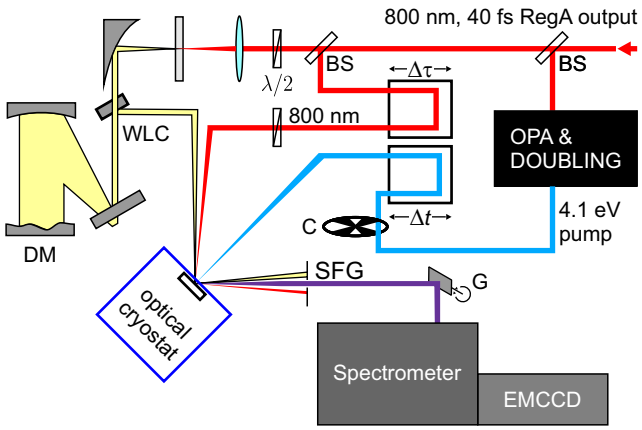

Figure 2. Experimental setup: see text for description. BS, beam splitter; $\lambda/2$, half-wave waveplate; DM, deformable mirror; $\Delta\tau$, delay stage for 800 nm - WLC delay; Δt, pump-probe delay stage; C, optical chopper; G, galvanometer mirror.

the pump: An optical parametric amplifier (OPA) produces 2.05 eV photons, which are frequency-doubled to achieve $\hbar\omega_{\text{pump}} = 4.1\,\text{eV}$. The WLC, ranging from 1.77 to 2.48 eV, is generated by focusing 5 % of the RegA output power into a 3 mm thick sapphire crystal, after rotating it to s-polarization with a $\lambda/2$ waveplate. As the group velocity dispersion of light increases with increasing frequency and therefore a broadband visible pulse is more strongly dispersed in time than a broadband IR pulse, time-dependent eSFG[20] is challenging compared to vSFG. To overcome this limit to the temporal resolution, we compress the WLC with a deformable mirror as described in Ref. 23. The remaining 800 nm light is filtered and used as upconverting beam, with either s- or p-polarization. The relative time delay $\Delta\tau$ between the WLC and the 800 nm beam, called the *fundamental* beams in the following, as well as the time delay Δt between the resulting eSFG field and the pump pulse are controlled by changing the optical path of the beams with motorized delay stages.

Both samples are simultaneously kept under vacuum conditions (1×10^{-7} mbar) in an optical continuous flow cryostat (Oxford instruments Optistat CV-F) and are cooled down to 100 K. The ZnO is cut along the non-polar $(10\bar{1}0)$ surface and oriented such that the c-axis is parallel to s-polarized light. The WLC impinges the sample at 45° along a plane that is parallel to the laser table and is focused with a spherical mirror of 250 mm focal length. The 800 nm upconverting beam forms a 1° angle with the WLC beam and is focused with a 300 mm focal length lens. Lastly, the pump beam is hitting the sample at normal incidence along the horizontal and at 45° along the vertical axis. This way, it is possible to geometrically block the scattered pump light before reaching the detector. The resulting eSFG beam, with energy ranging from 3.32 to 4.03 eV, is emitted between the reflected fundamental beams due to momentum conservation. All three beams are recollimated with a 100 mm focal length lens and the fundamental beams are used as a guide to align the eSFG output into the spectrometer. Scattered light of the fundamental beams and the second harmonic of the 800 nm beam are blocked by mechanical slit which only allows the eSFG to pass through. A short pass spectral filter transmitting between 3.28 and 3.95 eV (Semrock FF01-390/SP-25) is used to further block both the visible beams and the scattered pump light. The multicolor eSFG signal is dispersed into a spectrometer (Andor Shamrock 303i) and detected with an electron multiplying charge coupled device (EMCCD - Andor Newton A-DU970P-BV). The spectrometer is equipped with a 300 l/mm grating blazed at 300 nm, which allows the measurement of the whole wavelength range on the 1600 pixel detector. The energy resolution is set by the width of the upconverting pulse to be 66 meV, well above the 6.3 meV limit of the spectrometer in this energy range.

Before being focused onto the detector, the SFG beam is sent to a galvanometer mirror oscillating at a frequency of 500 Hz. An optical chopper in the pump beam is syn-

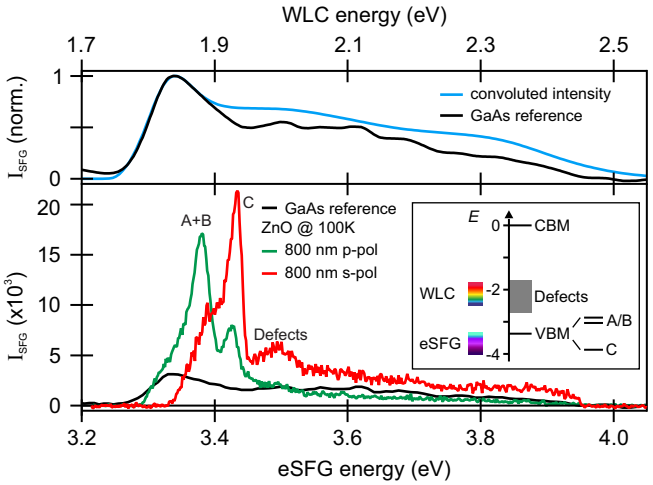

Figure 3. (Top) eSFG spectrum of GaAs (black) compared to the convolution of WLC and 800 nm spectrum (light blue) that defines the expected non-resonant eSFG spectrum. The eSFG response of GaAs shows no resonances in this region and is used as reference. (Bottom) eSFG spectrum of ZnO for two polarizations of the upconverting beam, p-polarized in green and s-polarized in red. In black for comparison the eSFG spectrum of GaAs (p-polarized 800 nm). Clearly the two ZnO eSFG spectra differ from the reference spectrum, exhibiting two strong resonances around 3.4 eV.

chronized with the galvanometer mirror such that it is possible to measure the pumped and unpumped eSFG spectra simultaneously as two vertically separated stripes on the detector. As mentioned above, the WLC is compressed to 20 fs with a deformable mirror. Despite the compression, the wavelength components of the WLC close to the edges of the mirror, where the membrane cannot deform, retain a slight temporal spread. This results in a difference between the eSFG spectrum at a given time delay $\Delta\tau$ between the fundamental pulses. Thus, the spectrum is integrated over the whole crosscorrelation, as shown in the supplementary online material[24]. To avoid loosing any relevant spectral information, for each pump-probe delay Δt the upconverting pulse is scanned at a constant velocity with respect to the WLC over a 160 fs range in $\Delta\tau$. This currently defines the time-resolution of the experiment.

The intensity of the upconverting beam cannot be increased arbitrarily, as unwanted dynamics could be triggered by multiphoton absorption. Indeed, as shown in the supplementary online material[24], we observe a nonlinearity in the transient reflectivity due to dynamics associated to the multiphoton absorption of 800 nm light at a power of 40 mW, corresponding to an incident fluence of 3.66 mJ cm^{-2}. To avoid this effect, the experiments were performed at 20 mW, corresponding to a fluence of 1.83 mJ cm^{-2}, in the regime where the transient reflectivity traces reflect the cross correlation of the fundamental pulses.

The non-resonant eSFG spectral shape can be estimated by the convolution of the spectra of the WLC and the 800 nm upconverting pulse and is plotted in light blue in the upper panel of Fig. 3. This spectral shape is the one expected for a material that does not have resonances at either the WLC, the upconverting or the eSFG photonenergies, as in the case of GaAs. Indeed, the GaAs spectrum (in black) is in good agreement with this prediction. From the band structure of ZnO, schematically summarized in the inset, we expect three final state resonances, i.e resonant with the sum frequency $\omega_1 + \omega_2$: Resonance A at 3.371 eV, B at 3.378 eV and C at 3.418 eV, arising from the crystal field splitting of the valence bands. Additionally, defect-related in-gap states (IGS) in the energy range between 1.7 and 2.7 eV below the conduction band minimum should lead to intermediate state resonances, i.e. resonant with the WLC only. The static resonant broadband eSFG response of ZnO at 100 K is plotted in the lower panel for the two different polarizations of the 800 nm beam (green, p-polarized and red, s-polarized) in comparison to the GaAs reference. Unlike GaAs, ZnO clearly shows a broad peak around 3.37 eV, visible only for p-polarization, i.e. when the field is perpendicular to the c-axis, and a narrower one at 3.43 eV, observed for both polarizations. We assign the low-energy resonance to contributions from both valence bands A and B and the high-energy one to valence band C. The energy positions and the polarization dependence are in good agreement with the exciton-polariton lines observed in reflectivity experiments[22]. Thus, we show that eSFG is sensitive to all band-edge resonances of ZnO. Additionally, a broad feature is observed in the s-polarized spectrum at energies above 3.45 eV, while the p-polarized spectrum coincides with the GaAs response. Corresponding to a resonant photon energy of around 2.0 eV, this broad feature is probably resulting from the IGS.

The non-equilibrium dynamics associated to these resonances after photoexcitation across the band gap, acquired in the s-polarized configuration, are shown in Fig. 4 (a) and represent the proof of principle of time-resolved electronic sum-frequency generation. The corresponding static eSFG spectrum (no pump) and the luminescence background due to the UV pumping only are plotted in the left panel in green and blue, respectively, as a function of eSFG (left axis) and WLC (right axis) energy in the left panel. The other panels show the pump-induced eSFG changes in false colors as a function of pump-probe delay Δt (bottom axis) after photoexcitation at 4.1 eV. Note that the figure displays raw data. Clearly, dynamics are visible at the eSFG resonance at 3.43 eV (361 nm), corresponding to the exciton C, and also at 3.38 eV (367 nm), the energy associated with the valence band resonances A and B that were not visible in the static spectrum.

Panel (b) compares exemplary eSFG spectra integrated over two selected delay ranges, indicated by the colored boxes in panel (a), and the static background $I_{BG}(E)$ which is the sum of the eSFG and the lumin-

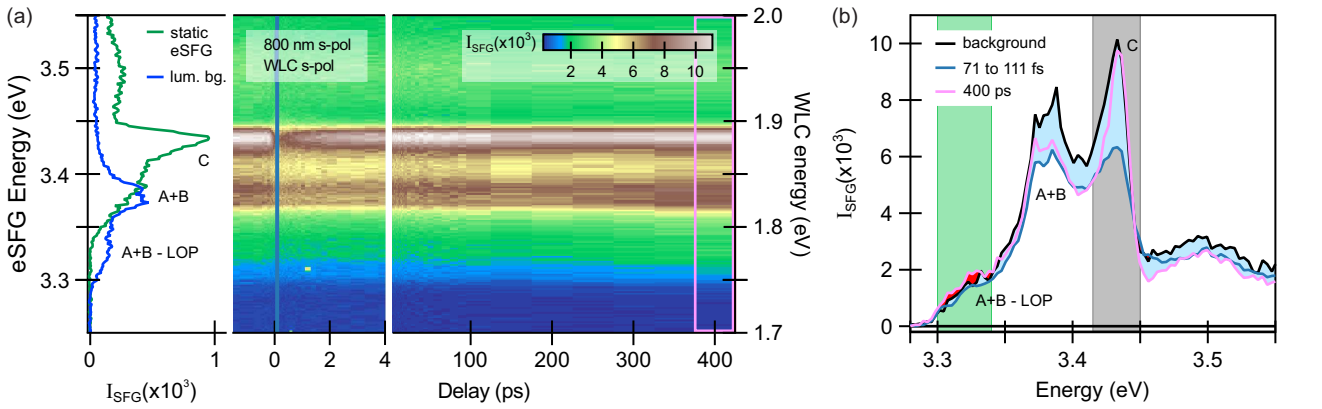

Figure 4. (a) Proof of principle of time-resolved electronic sum frequency generation. Left: Static eSFG and luminescence spectrum of ZnO, constituting the static background. Right: False color plot of the tr-eSFG intensity at 100 K as a function of eSFG energy (vertical) and the pump-probe delay (horizontal). Dynamics are clearly visible at the eSFG resonance C and at the maximum of the luminescence (3.38 eV, A+B). (b) eSFG variation for two selected pump-probe delays, corresponding to the colored rectangles in panel (a), with respect to the background (black) given by the sum of the static eSFG spectrum and the luminescence.

escence spectra depicted on the left of panel (a). The spectra have been binned in wavelength, such that each data point is averaged over two EMCCD pixels. For both time delays the traces clearly show (i) a negative variation, indicated by the blue shadow, while (ii) an additional positive variation (red shadow) is visible at the low energy shoulder for longer time delays. Quantitatively, the eSFG variation is defined as

$$\frac{\Delta I_{\mathrm{eSFG}}(\Delta t, E)}{I_{\mathrm{BG}}(E)} = \frac{I_{\mathrm{eSFG}}(\Delta t, E) - I_{\mathrm{BG}}(E)}{I_{\mathrm{BG}}(E)} \quad , \qquad (2)$$

where $I_{\mathrm{eSFG}}(\Delta t, E)$ is the measured eSFG intensity for a given delay Δt. A maximum negative average variation (i) of -30 % at time zero and a minimum variation of -3 % after 400 ps are observed for the resonant eSFG peak at 3.43 eV and calculated by averaging the eSFG intensity in the interval between 3.415 and 3.45 eV indicated by the grey box. The positive variation (ii) at the low-energy peak is quantified by integrating over the interval between 3.30 and 3.34 eV (green box), and, due to the width of the peak, results in an average 0.6 % variation per pixel. This constitutes the smallest I_{eSFG} variation we are able to resolve. The comparably fast dynamics (i) are assigned to the charge carrier relaxation in the bands, whereas the significantly slower signal increase (ii) is related to the formation of the excitonic ground state. A detailed discussion of the underlying physics goes beyond the scope of this Letter and will be presented in a forthcoming publication[25].

In summary, we have presented a setup for time-resolved electronic sum-frequency generation based on a compressed white light supercontinuum, with 160 fs time and 66 meV energy resolution. The broadband probing allows for the mapping of a wide range of electronic transitions at once, as demonstrated for the excitonic resonances of non-centrosymmetric ZnO. We showed that eSFG is sensitive to all band-edge resonances with symmetry specificity and is able to resolve time-dependent variations as small as 0.6 % per pixel. This data set is the proof of principle that time-resolved electronic sum frequency generation can unveil electronic resonances and their dynamics also in solid state compounds and constitutes the first step towards interface-selective time-resolved electronic spectroscopy.

We acknowledge fruitful discussions with K. Campen, S. Wall, and A. Melnikov. This project was partially funded by the Deutsche Forschungsgemeinschaft through Sfb 951.

REFERENCES

[1] R. W. Boyd, *Nonlinear Optics*, 3rd ed. (Elsevier Academic Press, 2008).
[2] P. Butcher and D. Cotter, *The elements of nonlinear optics* (Cambridge University Press, 1990).
[3] Y. R. Shen, *The principles of nonlinear optics* (John Wiley & sons, 1984).
[4] R. M. Corn and D. A. Higgins, Chemical Reviews **94**, 107 (1994), http://dx.doi.org/10.1021/cr00025a004.
[5] D. Zimdars, J. I. Dadap, K. B. Eisenthal, and T. F. Heinz, Chemical Physics Letters **301**, 112 (1999).
[6] T. F. Heinz, H. W. K. Tom, and Y. R. Shen, Phys. Rev. A **28**, 1883 (1983).
[7] A. L. Harris, L. Rothberg, L. H. Dubois, N. J. Levinos, and L. Dhar, Phys. Rev. Lett. **64**, 2086 (1990).
[8] A. Castro, E. V. Sitzmann, D. Zhang, and K. B. Eisenthal, The Journal of Physical Chemistry **95**, 6752 (1991).
[9] M. Morin, N. J. Levinos, and A. L. Harris, The Journal of Chemical Physics **96**, 3950 (1992).
[10] Y. Liu, J. I. Dadap, D. Zimdars, , and K. B. Eisenthal*, The Journal of Physical Chemistry B **103**, 2480 (1999).
[11] V. Fomenko, C. Hurth, T. Ye, and E. Borguet, Journal of Applied Physics **91**, 4394 (2002).
[12] A. E. Jailaubekov, A. P. Willard, J. R. Tritsch, W.-L. Chan,

N. Sai, R. Gearba, L. G. Kaake, K. Williams, K. Leung, P. J. Rossky, and X. Y. Zhu, Nat. Mater. **12**, 66 (2013).
[13]M. S. Yeganeh, J. Qi, A. G. Yodh, and M. C. Tamargo, Phys. Rev. Lett. **68**, 3761 (1992).
[14]W. Daum, H.-J. Krause, U. Reichel, and H. Ibach, Phys. Rev. Lett. **71**, 1234 (1993).
[15]A. Rubano, M. Fiebig, D. Paparo, A. Marino, D. Maccariello, U. Scotti di Uccio, F. Miletto Granozio, L. Marrucci, C. Richter, S. Paetel, and J. Mannhart, Phys. Rev. B **83**, 155405 (2011).
[16]A. Keens and H. Happ, Journal of Physics C **21**, 1661 (1988).
[17]S. W. Liu, J. Chakhalian, M. Xiao, and C. L. Chen, Applied Physics Letters **90**, 042901 (2007).
[18]C. Hess, M. Wolf, S. Roke, and M. Bonn, Surface Science **502 - 503**, 304 (2002).
[19]R. A. Livingstone, Y. Nagata, M. Bonn, and E. H. G. Backus, Journal of the American Chemical Society **137**, 14912 (2015).
[20]S. Yamaguchi and T. Tahara, Laser & Photonics Reviews **2**, 74 (2008).
[21]S. Yamaguchi and T. Tahara, The Journal of Physical Chemistry B **108**, 19079 (2004).
[22]D. Thomas, J. Phys. Chem. Solids **15**, 86 (1959).
[23]D. Wegkamp, D. Brida, S. Bonora, G. Cerullo, J. Stähler, M. Wolf, and S. Wall, Appl. Phys. Lett. **99**, 101101 (2011).
[24]See supplementary online material available at.
[25]L. Foglia, S. Sadofev, S. Blumstengel, and J. Stähler, (2016), in preparation.

SUPPLEMENTARY ONLINE MATERIAL

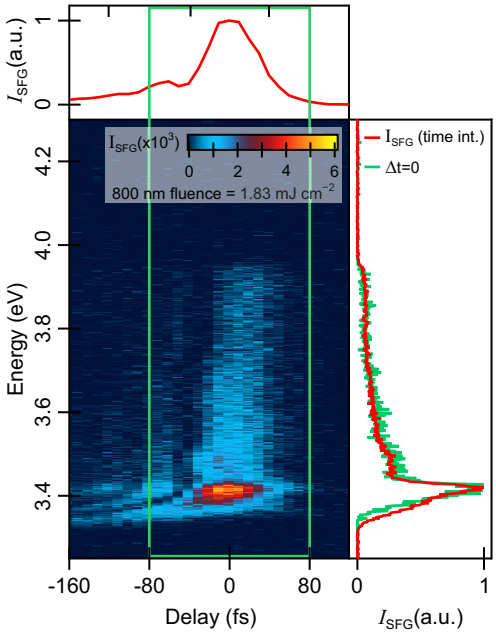

Figure 1. eSFG 2D intensity of ZnO as a function of energy (vertical) and time delay $\Delta\tau$ between the WLC and the 800 nm beam (horizontal). The spectrum clearly shows replicas in time attributed to the cutting of the WLC spectrum at the edge of the deformable mirror. Additionally, the low-energy edge is strongly affected by the uncompressed red edge of the WLC, due to the fixed edge of the mirror membrane. This results in different spectra for different delays $\Delta\tau$. (Right) eSFG spectra acquired at a fixed delay $\Delta\tau = 0$ (green) and integrated over the range $-80\,\text{fs} \leq \Delta\tau \leq 80\,\text{fs}$ (red). The two spectra clearly differ in the low-energy range. Since this energy range corresponds to the excitonic resonances discussed in the paper, it is not sufficient to acquire eSFG data at a fixed delay only, but the eSFG spectrum requires integration over the whole crosscorrelation of WLC and 800 nm. (Top) Spectrally integrated eSFG response as a function of delay $\Delta\tau$. The main peak exhibits a full width at half maximum of 61 fs, in good agreement with the temporal convolution of the 40 fs long 800 nm pulse and the 20 fs WLC.

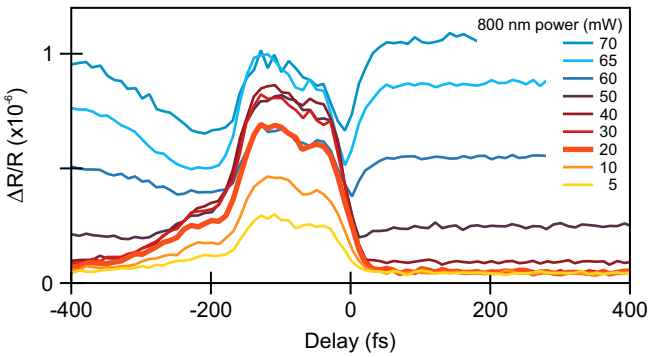

Figure 2. Dependence of the transient reflectivity of ZnO over the integrated WLC energy on the 800 nm pulse fluence. Starting at 40 mW, the data clearly show a non-linearity in the response at both positive and negative delays. This non-linearity is indicative of the onset of multiphoton absorption processes that lead to the creation of electronic excited state population by the upconverting pulse. At lower pulse energies instead, the ZnO response is comparable to the cross-correlation of the WLC and 800 nm pulses (taking into account the artefacts discussed in Fig. 1 of the SOM) and reflects only a change in the sample polarization but not the creation of an electronic population.